Chaotic dynamics on exceptional surfaces

Lei Chen,[*] Wenhao Wu, Feifan Huang ⓘ, Yaofei Chen, Gui-Shi Liu, Yunhan Luo,[†] and Zhe Chen

*Guangdong Provincial Key Laboratory of Optical Fiber Sensing and Communications, College of Science and Technology,
Jinan University, Guangzhou 510632, China
and Key Laboratory of Optoelectronic Information and Sensing Technologies of Guangdong Higher Education Institutes,
Jinan University, Guangzhou 510632, China*

Due to strong photon-phonon interaction, coupled microcavities have provided a fruitful platform for chaos investigation. In particular, the parity-time symmetric microcavities pair has attracted unprecedented attention since the exceptional point (EP) in the non-Hermitian system offers more intriguing and abundant dynamics. Motivated by achieving a robust EP, a novel exceptional surface (ES) notion is proposed in the coupled microcavities. However, the chaotic dynamics on the ES remain yet unexplored. This study explores the chaos generation on the ES. We discover that the ES could dramatically decrease the threshold of chaos generation by >50% compared to the eigenvalues escaping from the ES. Unlike conventional chaotic dynamics, chaotic signals on the ES possess a surprising globally flattened, but locally chirped spectrum. Such an advantage provides an additional degree of freedom to implement chaotic applications on the physical layer. In addition, a coupling phase-induced chaos is found, which demonstrates an accumulated chaos generation beyond the conventional wisdom. More importantly, such an arrangement enables chaotic signals to achieve the temporal Vernier and harmonic Vernier effects, expanding the scope of chaos. This study of chaos generation on the ES further stimulates applications in compact chaotic devices and potentially facilitates fundamental chaotic dynamics research.

Introduction. Chaotic systems are usually characterized by irregular dynamics, exponential sensitivity to initial conditions, and ergodicity of a typical trajectory in phase space. Benefiting from these advantages, the light in chaos has facilitated numerous applications, including secret and private communications [1,2], high-speed calculation [3,4], random number generation [5], microscopy imaging [6], and broadband optical devices [7]. Meanwhile, these features have also promoted the forefront of scientific research ranging from decoherence suppression [8] and synthetic dimension [9] to switchable bandpass and band-stop chaotic emission [10] and nonreciprocal propagation [11]. In recent years, the developed nanofabrication technology in a microcavity has significantly increased the Q-factor, and this advantage induces powerful radiation pressure, meriting extensive nonlinear interaction between the photon and phonon [12,13]. Consequently, the exploration of chaotic dynamics has begun to focus on more compact microcavities and opens the possibility of the chaotic generator on the chip [14,15].

Photon coupling between two microcavities has attracted much interest since its value determines the exceptional point (EP) [16,17]. The EP is a branch point singularity that arises in non-Hermitian physics [18]. It switches the phase transition between the parity-time (PT) symmetry-breaking phase and PT-symmetric phase [19,20], benefiting the applications from sensing technologies [21–23] to quantum computing [24,25].

Generally, an EP exists in a balanced gain and loss configuration [26]. However, this arrangement is challenging to maintain because it is insufficient to ensure energy conservation [27]. In addition, the optical gain introduces the heat reservoir's noise [28–30], which may destroy the quantum coherence. As a result, the alternative passive PT-symmetric structures were proposed to achieve a robust EP, such as in the nonlinear medium [31] or two coupled waveguides with different losses [30]. Nevertheless, an accurately equivalent balanced gain and loss pair apply a stringent requirement to form the EP, and therefore fabrication errors or perturbations may experimentally hinder an available EP.

Motivated by engineering a robust EP, a new notion was proposed, namely, the exceptional surface (ES) [32]. In theory, the system eigenvalues always take the degenerated EPs pair if its Hamiltonian possesses Jordan fashion [32,33]. Consequently, all EPs compose a hypersurface ES embedded in high-dimensional parameter space. Similar to the effect of topological protection, this new design generates a robust EP against fabrication errors or perturbation. In experiments, we can achieve an ES if the light couples from one microcavity to another in one way instead of reciprocal coupling. Because of the simplified optical design, the notion of ES has taken necessary steps forward to the robust microcavity laser and sensing application.

The current study explores the chaos generation on the ES. We discovered that the ES could dramatically decrease the threshold of chaos generation by >50% compared to the reciprocal coupling situation. Unlike conventional chaotic dynamics, chaotic signals on the ES possess a surprising

---

[*]Corresponding author: chenlei@jnu.edu.cn
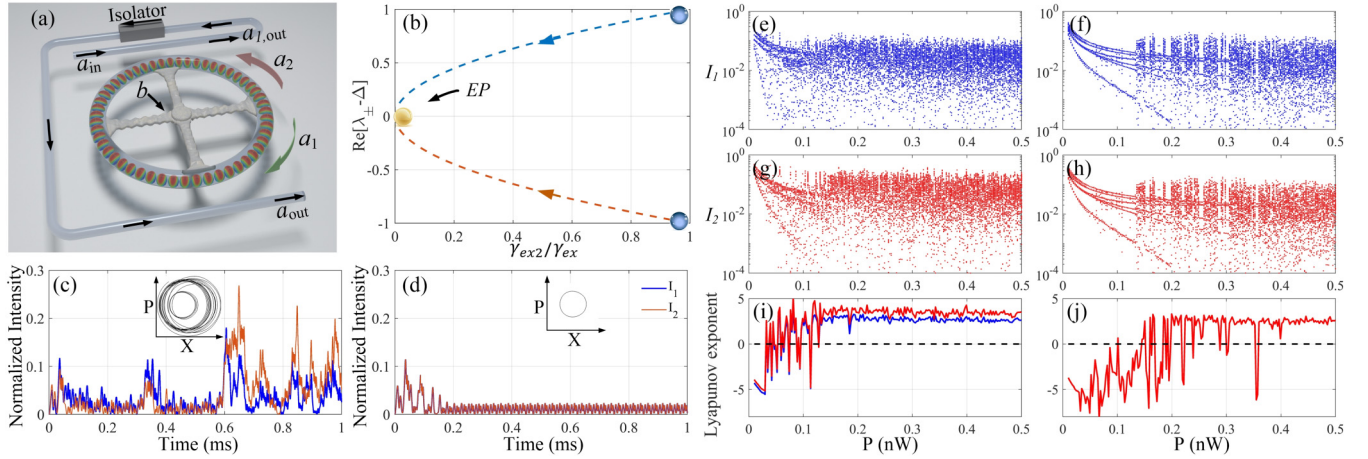[†]Corresponding author: yunhanluo@163.com

FIG. 1. (a) Scheme of the chaos generation on the ES. (b) Calculated real part of eigenvalues with reciprocal coupling (blue) and one-way coupling $a_1 \rightarrow a_2$ (orange), where γ_{ex2} indicates the coupling strength of $a_2 \rightarrow a_1$; $\theta = 0$; $J = 0$. Evolutions of I_1 and I_2 with (c) one-way and (d) reciprocal coupling when $P = 0.3$ nW. Insets in (c) and (d) show two trajectories of the mechanical motion from 0.5 to 1 ms. Bifurcation diagrams of I_1 vs P with (e) one-way and (f) reciprocal coupling. Bifurcation diagrams of I_2 vs P with (g) one-way and (h) reciprocal coupling. The Lyapunov exponent of I_1 and I_2 vs the power of light input with (i) one-way and (j) reciprocal coupling.

globally flattened, but locally chirped spectrum. Such an advantage provides an additional degree of freedom to implement chaotic applications on the physical layer. In addition, a coupling phase-induced chaotic dynamic is found, which demonstrates an accumulated chaos generation beyond the conventional wisdom. More importantly, such an arrangement enables chaotic signals to access the temporal Vernier and harmonic Vernier effects by controlling the coupling of two optical modes. Our study of chaos generation on the ES potentially progresses the fundamental chaotic dynamics and further stimulates applications in compact on-chip chaotic devices.

Theoretical model and analysis. We used the scheme in Fig. 1(a) to achieve an experimentally accessible ES. The light input a_{in} generates the microcavity mode a_1, and their output $a_{1,out}$ stimulates the microcavity mode a_2. In terms of the optomechanical system coupling to the microcavity, the hybrid system Hamiltonian can be described by

$$H = H_0 + H_p + H_m - i\hbar\Omega_d \sum_{j=1,2}(a_j^\dagger - a_j), \quad (1)$$

where $H_0/\hbar = \Delta \sum_{j=1,2} a_j^\dagger a_j + \widetilde{\gamma_{ex}} a_1 a_2^\dagger$ with the note of $\widetilde{\gamma_{ex}} = \gamma_{ex} e^{i\theta}$, $H_p/\hbar = J(\sum_{j=1,2} a_j^\dagger a_j + a_1 a_2^\dagger + a_1^\dagger a_2)$, and $H_m/\hbar = \omega_m b^\dagger b - g \sum_{j=1,2} a_j^\dagger a_j (b^\dagger + b)$. The terms of $a_j(a_j^\dagger)$ and $b(b^\dagger)$ are the annihilation (creation) operators of the optical modes and mechanical mode, respectively. The microcavity is driven with frequency ω_d and amplitude $\Omega_d = \sqrt{P\gamma_{ex}/\hbar\omega_d}$, with the note of power P and coupling strength γ_{ex}; θ is the coupling phase; Δ is the detuning in a frame rotating with ω_d, i.e., $\Delta = \omega_c - \omega_d$ with the note of the angular frequency of microcavity ω_c; and J is the perturbation contributed by scattering on the microcavity. ω_m and g are the angular frequency of the mechanical mode and the coupling between the optical and mechanical modes, respectively. Note that the arrangement in Fig. 1(a), even without the isolator, has banned the coupling $a_2 \rightarrow a_1$ and only allowed the coupling $a_1 \rightarrow a_2$. As a result, it leads to the

Jordan-form Hamiltonian, and the system accesses the ES. However, two light paths can realize the coupling $a_1 \rightarrow a_2$, that is, $(\widetilde{\gamma_{ex}})^* a_1 a_2^\dagger$ and $\widetilde{\gamma_{ex}} a_1 a_2^\dagger$. Therefore, the coupling strength $a_1 \rightarrow a_2$ is sensitive to $\cos(\theta)$. Here, we inserted an isolator into the light path to constrain the light in one-way propagation to remove the sensitivity.

To explore the chaotic dynamics on the ES, we employed the semiclassical Langevin equations of motion. Taking into account the cavity dissipation and mechanical damping, the Lindblad master equations can be described as

$$\dot{x} = \omega_m p, \quad (2a)$$

$$\dot{p} = -\left(\frac{\gamma_m}{2}\right)p - \omega_m x + \sqrt{2}g\sum_{j=1,2}|a_j|^2, \quad (2b)$$

$$\dot{a}_1 = -i\left(\Delta + J - \frac{i\gamma}{2}\right)a_1 - iJa_2 + i\sqrt{2}ga_1x - \Omega_d, \quad (2c)$$

$$\begin{aligned}\dot{a}_2 = &-i\left(\Delta + J - \frac{i\gamma}{2}\right)a_2 - i(J + \gamma_{ex}e^{i\theta})a_1 \\ &+ i\sqrt{2}ga_2x - \Omega_d e^{i\theta},\end{aligned} \quad (2d)$$

where $x = (b^\dagger + b)/\sqrt{2}$ is the position operator of the mechanical mode and $p = i(b^\dagger - b)/\sqrt{2}$ is the momentum operator of the mechanical mode. To further gain physical insight into the system dynamics on the ES, we calculated the eigenvalues without mechanical motion in Fig. 1(b). The microcavity modes access the ES when the light path allows the one-way light coupling $a_1 \rightarrow a_2$. As a result, the system eigenvalues generate a degenerated pair, as the orange dot shows in Fig. 1(b). In contrast, when the light is allowed to reciprocal coupling from one microcavity mode to the other, i.e., assuming $H_0/\hbar = \Delta \sum_{j=1,2} a_j^\dagger a_j + \widetilde{\gamma_{ex}} a_1 a_2^\dagger + \widetilde{\gamma_{ex2}} a_1^\dagger a_2$, the system eigenvalues are separated, as the blue dots show in Fig. 1(b).

To highlight the physical feature on the ES, we selected a microcavity with a high-quality Q-factor $\sim 2.4 \times 10^{10}$ in the calculation, Specifically, $\omega_c = 1216$ THz, corresponding to 1550 nm, $\omega_m = 40$ kHz, $\omega_d = \omega_c - \omega_m$, $\gamma = \gamma_c + \gamma_{ex}$
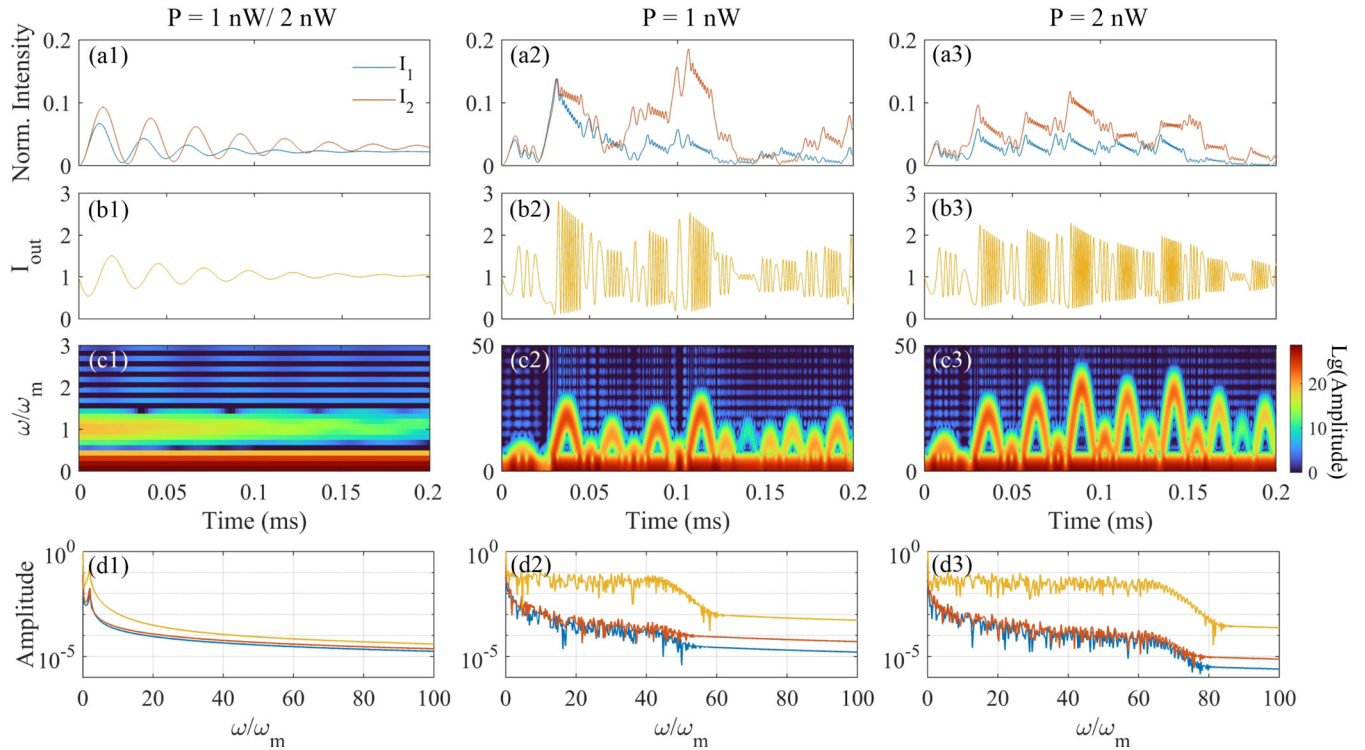
FIG. 2. Dynamics of I_1 and I_2 (a1) in the absence of mechanical mode, and considering mechanical mode with light input of (a2) 1 nW and (a3) 2 nW. (b1)–(b3) The light output under the corresponding situations of (a1)–(a3). (c1)–(c3) STFT under the corresponding situations of (a1)–(a3). (d1)–(d3) Fourier transform under the corresponding situations of (a1)–(a3).

with the note of microcavity decay rate $\gamma_c/2\pi = 2$ kHz and $\gamma_{ex}/2\pi = 6$ kHz, $\gamma_m/2\pi = 1$ kHz, $g/2\pi = 0.5$ kHz. More physically accessible parameters can be found in Refs. [34–36]. Without loss of generality, we take $\theta = 0$ and $J = 0$ in this part. Because of the contribution of ES, the light intensities and the mechanical motion in phase space access chaotic dynamics in Fig. 1(c), when we stimulate the arrangement in Fig. 1(a). However, if we allowed the light reciprocal coupling, the identical light input generates chaotic dynamics initially but quickly converts to periodic dynamics, as shown in Fig. 1(d). The inset in Fig. 1(d) presents the phase space of the mechanical oscillation, and the circle indicates a perfect periodic behavior.

To verify the ES decreased threshold in chaos generation, we calculated the bifurcation diagrams of I_1 and I_2 versus the power of light input with one-way coupling in Figs. 1(e) and 1(g) and with reciprocal coupling in Figs. 1(f) and 1(h), respectively. Figures 1(f) and 1(h) demonstrate several distinguished lines if the power is less than ~ 0.15 nW, showing periodic dynamics. Then the system requires a relatively broad power supply from ~ 0.15 to ~ 0.35 nW for intermittent chaos, suggesting a relatively weak nonlinear interaction. However, an EP may contribute a stronger photon-phonon interaction because of the non-Hermitian uniqueness [27]. Therefore, the distinguished curves in Figs. 1(e) and 1(g) are quickly vanished and blend into the chaotic environment. Meanwhile, their corresponding Lyapunov exponent curves in Figs. 1(j) and 1(i) have also manifested their different chaotic paths, verifying the decreased threshold in chaos generation on the ES.

Result and discussion.

A. Light output on the ES. To obtain the output on the ES, we calculated the I_{out} regarding the interference of three components, i.e., a_1, a_2, and light input,

$$I_{out} \equiv |a_{out}|^2 = \left| e^{i\theta} + \frac{\gamma_{ex}}{\Omega_d} a_1 e^{i\theta} + \frac{\gamma_{ex}}{\Omega_d} a_2 \right|^2. \quad (3)$$

To highlight the photon-phonon interaction, we first present the light dynamics without mechanical motion as a reference. Due to the lack of photon-phonon interaction, the modes in the optical microcavity describe a linear system. Thus, I_1 and I_2 in Fig. 2(a1) present the damped oscillations, resulting in a damped dynamic in I_{out} in Fig. 2(b1). In addition, the linear system features an independent power of light input. In contrast, the most peculiar signature is power-dependent light dynamics because of photon-phonon interaction. When $P = 1$ or 2 nW, the dynamics of the microcavity modes are different compared to Figs. 2(a2) and 2(a3). Consequently, Figs. 2(b2) and 2(b3) show that I_{out} is highly dependent on P in the chaotic regime.

In addition, the local oscillated frequency changes remarkably in the chaotic regime on the ES. To evaluate the rapidly changing spectra, we implemented the short-time Fourier transform (STFT) to Figs. 2(b1)–2(b3) and show the results in Figs. 2(c1)–2(c3). As a reference, Fig. 2(c1) shows that the oscillation frequency is unchanged in a linear system. However, the oscillation frequency in the chaotic regime varies with a parabolic fashion, which indicates a chirped dynamic. In principle, the sharply changed light intensity merits the large dispersion according to the Kramers-Krönig
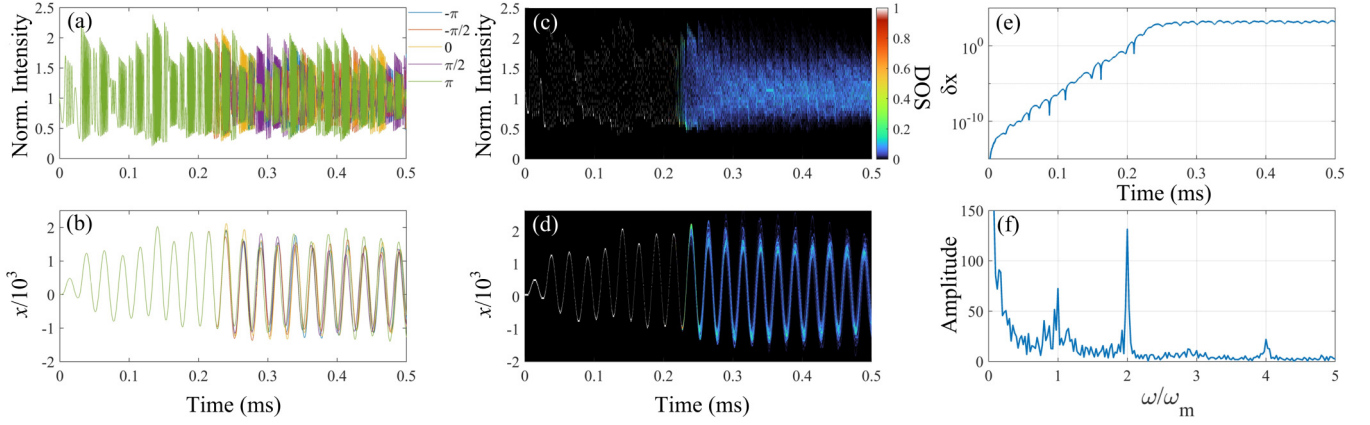
FIG. 3. (a) I_{out} and (b) x with five typical phases when $P = 2$ nW. DOS of (c) I_{out} and (d) x. (e) Variation of δx vs time. (f) FT of δx.

relation [37]. In this manner, the rectangularlike pluses in chaotic signals result in chirped dispersion. Therefore, when two microcavity modes interfere, the output in Eq. (3) generates a chirped dynamic, providing an additional degree of freedom to manipulate the chaos. Also, benefiting from the stronger photon-phonon interaction, a powerful light input on the ES anticipates a higher local oscillation frequency, comparing Figs. 2(c2) and 2(c3), and broader spectrum, comparing Figs. 2(d2) and 2(d3). More importantly, compared to the conventional chaotic dynamics, I_{out} on the ES shows a more flattened spectrum due to the unchanged offset induced by interference. Such an advantage is highly in demand for applications such as random number generations and communications.

B. Coupling phase-induced chaos. The output on the ES associated with system variable θ shows a feature beyond the conventional wisdom in chaos generation. Specifically, if a chaotic system evolves along highly different trajectories, different initials or different system variables may contribute to the difference. In the first aspect, although slightly different initials in a chaotic system may yield highly different trajectories, the difference mainly focuses on long-time unpredictable behavior instead of from the beginning. In the second aspect, if a system variable changes, the states change from the beginning for slightly different initials or even identical initials in contrast. Here, θ in Fig. 1(a) is a system variable rather than initials, but the output shows a strikingly long-time unpredictable behavior after ∼0.2 ms for different θ from 0 to 2π instead of generating a difference at the beginning. We show five typical dynamics of I_{out} and their corresponding mechanical amplitudes in Figs. 3(a) and 3(b) to exhibit this unusual result.

Motivated by understanding this unusual mechanism, we calculated the density of state (DOS) of the light output I_{out} in Fig. 3(c) and mechanical amplitude x in Fig. 3(d), respectively. The DOS for I_{out} and x approach 100% at the beginning, independent of θ, and then the occupied state for both gradually spreads after ∼0.2 ms. Note that the DOS of I_{out} possesses an aperiodic variation in Fig. 3(c). Meanwhile, the DOS of x produces a significant variation around poles compared to the relatively small variation around the zero-crossing points in Fig. 3(c). This phenomenon indicates that due to loop configuration, the complex nonlinear response of x

plays an essential role in DOS. The loop configuration allows a_1 to stimulate a_2, and the mechanical oscillator mediates a_1 and a_2. Such a process enables a_2 to impact a_1, equivalently changing the initials.

Then, we focus on the variation of the mechanical mode x in Fig. 3(e) to confirm its complex nonlinear response. The trajectory variation grows overall from the beginning with a nearly exponential increment, which is consistent with the assumption of exponential growth in chaotic dynamics because of slightly different initials. However, a noticeable feature of the curve is that the variation possesses an oscillated behavior in Fig. 3(e), indicating the variation may sharply decrease. Then, we carried out Fourier transform (FT) to Fig. 3(e) to achieve its mode components. The result in Fig. 3(f) clearly shows that the spectral variation mainly originates from the harmonics of x, which verifies the complex nonlinear response.

C. Chaos in temporal Vernier and harmonic Vernier effects. Due to composing of EPs, the most intriguing application of ES is the ultrasensitive system feature near the hypersurface. Regardless of the mechanical oscillation, if a scatter penetrates the microcavity's evanescent field, the system Hamiltonian described by the quantum Rabi model possesses a parity (or Z_2) symmetry contributed by the coupling between two optical modes [38]. To be specific, system eigenvalues equal to $\Delta + J - i\gamma/2 \pm \sqrt{J(J + \gamma_{ex}e^{i\theta})}$ and such a discrete Z_2 symmetry generate the continuous U(1) symmetry in the dynamics [39], i.e., an alternate oscillation between I_1 and I_2. When the contribution of the mechanical oscillation is considered, we surprisingly find that although the dynamics of microcavity modes I_1 and I_2 are chaotic due to the photon-phonon interaction, their intensities alternate oscillation, as shown in Figs. 4(a1) and 4(a2), indicating the coexistence of U(1) symmetry and chaos.

Benefiting from the compatibility of the U(1) symmetry and chaotic dynamics, coupling J between a_1 and a_2 enables chaotic signals to achieve the Vernier and harmonic Vernier effects in the time dimension, as shown in Figs. 4(b1) and 4(b2). We zoomed in two typical time windows to highlight these effects in Figs. 4(c1) and 4(c2). Vernier and harmonic Vernier effects are two types of significant spectrum envelope modulation approaches [40]. These effects are usually formed by combining two interferences or resonators with similar or multiple free spectral ranges. Slightly different from the conventional Vernier and harmonic Vernier effects in
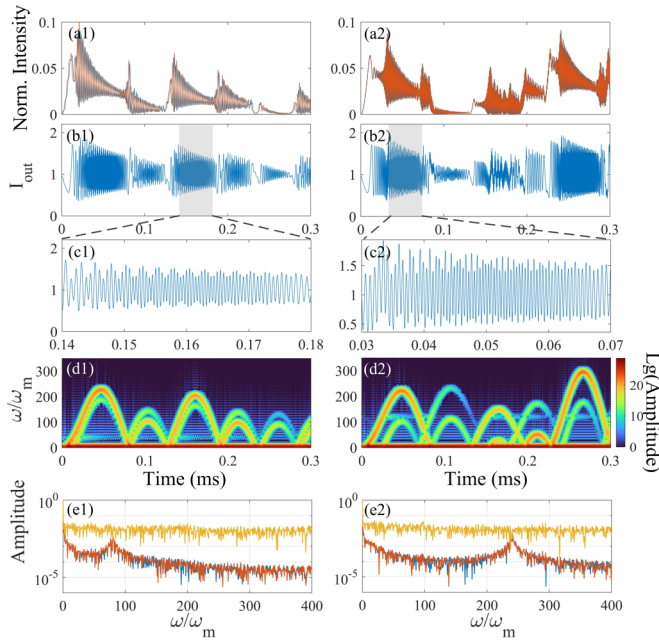
FIG. 4. . Dynamics of I_1 and I_2 with (a1) $J/2\pi = 200$ kHz and (a2) $J/2\pi = 600$ kHz, where $P = 2$ nW, $\theta = -\pi/2$, $\omega_m/2\pi = 10$ kHz. I_{out} in (b1) and (b2) corresponds to the situation of (a1) and (a2). (c1) and (c2) The enlarged details in (b1) and (b2), respectively. (d1) and (d2) The STFT results of (b1) and (b2). (e1) and (e2) The FT results of I_1, I_2, and I_{out}.

spectra, we present these effects in the time domain. However, the fundamental principle is attributed to the interference from three optical modes, identical to the conventional Vernier and harmonic Vernier effects in the spectra. Specifically, due to nonzero coupling J, a_1 and a_2 alternate oscillation, reflecting U(1) symmetry. Thus, the interference of three modes, i.e., a_1, a_2, and $a_{1,out}$, acts as the modulation in the time dimension, leading to the temporal Vernier and harmonic Vernier effects embedded in the chaotic dynamics.

We implemented the STFT to Figs. 4(b1) and 4(b2) to gain a more physical insight into the temporal Vernier and harmonic Vernier effects, as shown in Figs. 4(d1) and 4(d2). Due to the impact of dispersion, the chirped oscillation still holds compared to Figs. 4(b1) and 4(d1), but the mode components

have split in Fig. 4(d1), implying the Vernier effect. Then, a larger coupling J expands the gap, as shown in Fig. 4(d2). When the frequency of the upper mode is nearly twice that of the lower one, the harmonic Vernier effect happens compared to Figs. 4(c2) and 4(d2).

Notably, such a chaotic interference merits an excellent feature in the robust flattened spectrum, immune to coupling J. Because I_1 and I_2 alternate oscillation, their FTs show an observable peak embedded in the chaotic spectrum, as shown in Figs. 4(e1) and 4(e2). However, an exceptional phenomenon is that these peaks do not influence the spectra of I_{out} because of the changed offset. This robust property may help to progress the intensive applications relying on a flattened spectrum.

Conclusion. In summary, this work presented chaos generation on the ES. We discovered that the ES could dramatically decrease the threshold of chaos generation by $>50\%$. Compared to the conventional chaotic signals, the ES provides a more flattened chaotic spectrum similar to the white noise, but the more exciting signature is that these chaotic signals are locally chirped. Such a feature offers an additional degree of freedom to implement chaotic applications on the physical layer. In addition, a coupling phase-induced chaotic dynamic is found, which demonstrates an accumulated chaos generation beyond the conventional wisdom in chaos generation. More importantly, such an arrangement enables chaotic signals to access the temporal Vernier and harmonic Vernier effects in the time dimension, expanding the scope of chaos investigation. This study of chaos generation on the ES further stimulates applications in compact on-chip chaotic devices and potentially contributes toward progress in the fundamental research on chaos.

[1] L. Wang, X. Mao, A. Wang, Y. Wang, Z. Gao, S. Li, and L. Yan, Opt. Lett. **45**, 4762 (2020).

[2] O. Spitz, A. Herdt, J. Wu, G. Maisons, M. Carras, C.-W. Wong, W. Elsäßer, and F. Grillot, Nat. Commun. **12**, 3327 (2021).

[3] P. Antonik, M. Haelterman, and S. Massar, Phys. Rev. Appl. **7**, 054014 (2017).

[4] S. Kumar, J. P. Strachan, and R. S. Williams, Nature (London) **548**, 318 (2017).

[5] W.-Z. Yeoh, J. S. Teh, and H. R. Chern, Multimed. Tools. Appl. **78**, 15929 (2019).

[6] V. Anand, S. H. Ng, J. Maksimovic, D. Linklater, T. Katkus, E. P. Ivanova, and S. Juodkazis, Sci. Rep. **10**, 13902 (2020).

[7] X. Jiang, L. Shao, S.-X. Zhang, X. Yi, J. Wiersig, L. Wang, Q. Gong, M. Lončar, L. Yang, and Y.-F. Xiao, Science **358**, 344 (2017).

[8] F. Monifi, J. Zhang, Ş. K. Özdemir, B. Peng, Y.-X. Liu, F. Bo, F. Nori, and L. Yang, Nat. Photon. **10**, 399 (2016).

[9] M. Arnal, G. Chatelain, M. Martinez, N. Dupont, O. Giraud, D. Ullmo, B. Georgeot, G. Lemarié, J. Billy, and D. Guéry-Odelin, Sci. Adv. **6**, eabc4886 (2020).

[10] F. Huang, L. Chen, L. Huang, J. Huang, G. Liu, Y. Chen, Y. Luo, and Z. Chen, Phys. Rev. A **104**, L031503 (2021).

[11] D.-W. Zhang, L.-L. Zheng, C. You, C.-S. Hu, Y. Wu, and X.-Y. Lü, Phys. Rev. A **104**, 033522 (2021).

[12] T. Carmon, M. C. Cross, and K. J. Vahala, Phys. Rev. Lett. **98**, 167203 (2007).

[13] W. Noh, M. Dupré, A. Ndao, A. Kodigala, and B. Kante, ACS Photon. **6**, 389 (2019).

[14] L. Ge, Europhys. Lett. **123**, 64001 (2018).

[15] Z.-X. Liu, C. You, B. Wang, H. Dong, H. Xiong, and Y. Wu, Nanoscale **12**, 2118 (2020).

[16] M.-A. Miri and A. Alu, Science **363**, 6422 (2019).

[17] H. Jing, S. K. Özdemir, X.-Y. Lü, J. Zhang, L. Yang, and F. Nori, Phys. Rew. Lett. **113**, 053604 (2014).

[18] S. K. Özdemir, S. Rotter, F. Nori, and L. Yang, Nat. Mater. **18**, 783 (2019).

[19] M. Parto, Y. G. Liu, B. Bahari, M. Khajavikhan, and D. N. Christodoulides, Nanophotonics **10**, 403 (2021).

[20] X.-Y. Lu, H. Jing, J.-Y. Ma, and Y. Wu, Phys. Rev. Lett. **114**, 253601 (2015).

[21] W. Chen, S. K. Özdemir, G. Zhao, J. Wiersig, and L. Yang, Nature (London) **548**, 192 (2017).

[22] X. Mao, G.-Q. Qin, H. Yang, H. Zhang, M. Wang, and G.-L. Long, New J. Phys. **22**, 093009 (2020).

[23] J.-H. Park, A. Ndao, W. Cai, L. Hsu, A. Kodigala, T. Lepetit, Y.-H. Lo, and B. Kanté, Nat. Phys. **16**, 462 (2020).

[24] S. D. Sarma, M. Freedman, and C. Nayak, npj Quantum Inf. **1**, 15001 (2015).

[25] M. Pan, H. Zhao, P. Miao, S. Longhi, and L. Feng, Nat. Commun. **9**, 1308 (2018).

[26] B. Peng, Ş. K. Özdemir, F. Lei, F. Monifi, M. Gianfreda, G. L. Long, S. Fan, F. Nori, C. M. Bender, and L. Yang, Nat. Phys. **10**, 394 (2014).

[27] N. A. Mortensen, P. Goncalves, M. Khajavikhan, D. N. Christodoulides, C. Tserkezis, and C. Wolff, Optica **5**, 1342 (2018).

[28] C. M. Caves, Phys. Rev. D **26**, 1817 (1982).

[29] S. Scheel and A. Szameit, Europhys. Lett. **122**, 34001 (2018).

[30] F. Klauck, L. Teuber, M. Ornigotti, M. Heinrich, S. Scheel, and A. Szameit, Nat. Photon. **13**, 883 (2019).

[31] M.-A. Miri and A. Alu, New J. Phys. **18**, 065001 (2016).

[32] Q. Zhong, J. Ren, M. Khajavikhan, D. N. Christodoulides, Ş. K. Özdemir, and R. El-Ganainy, Phys. Rev. Lett. **122**, 153902 (2019).

[33] Q. Zhong, J. Kou, Ş. K. Özdemir, and R. El-Ganainy, Phys. Rev. Lett. **125**, 203602 (2020).

[34] E. Verhagen, S. Deléglise, S. Weis, A. Schliesser, and T. J. Kippenberg, Nature (London) **482**, 63 (2012).

[35] M. Aspelmeyer, T. J. Kippenberg, and F. Marquardt, Rev. Mod. Phys. **86**, 1391 (2014).

[36] V. Huet, A. Rasoloniaina, P. Guillemé, P. Rochard, P. Féron, M. Mortier, A. Levenson, K. Bencheikh, A. Yacomotti, and Y. Dumeige, Phys. Rev. Lett. **116**, 133902 (2016).

[37] V. Lucarini, J. J. Saarinen, K.-E. Peoponen, and E. M. Varti-ainen, *Kramers-Kronig Relations in Optical Materials Research* (Springer, Berlin Heidelberg, 2005).

[38] L. Chen and K. C. Chou, Photon. Res. **6**, 1003 (2018).

[39] Q. Bin, Y. Wu, and X.-Y. Lu, Phys. Rev. Lett. **127**, 073602 (2021).

[40] A. D. Gomes, M. S. Ferreira, J. Bierlich, J. Kobelke, M. Rothhardt, H. Bartelt, and O. Frazão, Sensors **19**, 5431 (2019).